NJC

Accepted Manuscript

This is an *Accepted Manuscript*, which has been through the Royal Society of Chemistry peer review process and has been accepted for publication.

Accepted Manuscripts are published online shortly after acceptance, before technical editing, formatting and proof reading. Using this free service, authors can make their results available to the community, in citable form, before we publish the edited article. We will replace this *Accepted Manuscript* with the edited and formatted *Advance Article* as soon as it is available.

You can find more information about *Accepted Manuscripts* in the Information for Authors.

Please note that technical editing may introduce minor changes to the text and/or graphics, which may alter content. The journal's standard Terms & Conditions and the Ethical guidelines still apply. In no event shall the Royal Society of Chemistry be held responsible for any errors or omissions in this *Accepted Manuscript* or any consequences arising from the use of any information it contains.

ROYAL SOCIETY OF CHEMISTRY

www.rsc.org/njc

Cite this: DOI: 10.1039/c0xx00000x

www.rsc.org/xxxxxx

ARTICLE TYPE

Facile shape control of nano-coaxial Co_3O_4/TiO_2 arrays and the effect of the microstructure on lithium storage capability

Tao Qi, Shichao Zhang,* Xiaomeng Wu, Yalan Xing, Guanrao Liu and Yanbiao Ren

Received (in XXX, XXX) Xth XXXXXXXXX 20XX, Accepted Xth XXXXXXXXX 20XX

DOI: 10.1039/b000000x

Arrays of self-supported core-shell nanowire have attracted considerable attention with respect to improved capability of electrochemical energy storage. Herein, we report a facile strategy, involving hydrothermal and liquid phase deposition (LPD) routes, to fabricate nano-coaxial Co_3O_4/TiO_2 arrays with intriguing morphologies, architectures, and chemical compositions. When tested as anode materials for lithium ion batteries, these nanohybrids have exhibited high reversible capacity, excellent cycling stability and good rate capability. It is assumed that the excellent electrochemical performance originates from the intricate core-shell nanoarchitecture and the coating effect of TiO_2, including improved mechanical/chemical stability and good strain accommodation. The improved lithium ion storage performance of Co_3O_4/TiO_2 nanostructure indicates its potential application as anode materials for electrochemical energy storage and the potential use of TiO_2 coating for modification of other anode materials.

Introduction

The development of next-generation Li-ion microbatteries demands to achieve high areal energy and power densities within the limited footprint area (e.g., <1 cm^2) because the characteristic allows it to be integrated with micro-electrochemical systems (MEMS) and to supply enough energy for them.[1-7] Among various active materials, nanostructured metal oxides with high capacity and low cost are especially attractive to advanced electrodes to meet those specific requirements of Li-ion microbatteries. In particular, Co_3O_4 with theoretical specific capacity (890mAh/g) and TiO_2 (335 mAh/g) are widely investigated as anode materials due to their earth-abundance and environmental friendliness.[5,17,35-37] However, poor cyclability and rate capability of Co_3O_4 as well as low capacity of TiO_2 greatly hinder their practical applications with sole institute.[5,6,17-19] To address these problems, an alternative strategy is to integrate Co_3O_4 and TiO_2 with a delicate structural design to improve the performance combining the strong points of the components. Although many Co_3O_4-based nanocomposites, such as CNTs@Co_3O_4[7,8], Graphene@Co_3O_4[9,10], and various one-dimensional heterostructures based on Co_3O_4 nanowires have been reported and investigated on their electrochemical performance.[11-13] To the best of our knowledge, the fabrication and Li^+ storage application of nanostructured Co_3O_4/TiO_2 electrode are rarely explored. In particular, Co_3O_4 nanowire arrays (NWs) have demonstrated their potential in improving lithium storage capability.[14-16] But their weaknesses, such as poor electronic conduction and fast capacity fading, will be prominent toughness as making them thicker for the purpose of storing more charge on limited footprint area. Moreover, considering a couple of concerns about the carbon coating, such as its layered structures being easily intercalated by solvent molecules, weak binding affinity to active materials, and poor thermal stability,[39] it is necessary to seek an alternative for carbon to be the surface. As a candidate material, TiO_2 stands out not only due to its small volume change, excellent cycling stability and rate capability but also due to its stable crystal structure to electrolyte and good thermal stability.[17-19] However, the conventional coating strategy for TiO_2 shell such as atomic layer deposition technique, seems to be costly and inconvenient.[26,38] Herein, for the first time, we report a cost-effective and facile strategy, involving hydrothermal and liquid phase deposition (LPD) routes,[26-28] to design and fabricate novel nano-coaxial Co_3O_4/TiO_2 heterostructures directly grown on Ti foil. As a binder free electrode for high-performance Li^+ storage application, Co_3O_4 NWs acts as the core and nanoscaled TiO_2 works as the shell layer. The presented nanoelectrode design offers several advantages as follows: First, Co_3O_4 nanowires with well-defined morphology can serve as both the backbone and conductive connection for TiO_2, and its porous and 1D structure with enlarged specific surface area, provides ideal electron pathway and load more active materials per unit electrode area.[33] Second, nanoscaled TiO_2 shell can increase the contact area with electrolyte, enable fast redox reaction, and most importantly, protect the inner structure of ultra-long Co_3O_4 nanowire core from collapse or even pulverization, leading to better cycling stability as well as long cycling endurance.[17-25,38] The synthesized nano-coaxial Co_3O_4/TiO_2 nanohybrids exhibit favorable electrochemical performance such as improved rate capability, high areal capacity

School of Materials Science and Engineering, Beijing University of Aeronautics and Astronautics, Beijing 100191, P R China; Fax: +86-10-82339319;Tel:+86-10-82338148;E-mail: csc@buaa.edu.cn

† Electronic Supplementary Information (ESI) available: Information about additional experimental data including FESEM images, CV curves, and electrochemical performances of the relevant electrodes or samples. See DOI: 10.1039/b000000x/

and long-term cycle stability in contrast with that of Co_3O_4 and TiO_2 component individually. Moreover, the morphology control of Co_3O_4/TiO_2 and correlations between electrochemical property and electrode morphology are also discussed.

Experimental

Preparation of Co_3O_4 NWs

Co_3O_4 NWs were synthesized by a hydrothermal method and subsequent calcination. In a typical synthesis, 1.630g cobalt nitrate ($Co(NO_3)_2{\cdot}6H_2O$), 0.415g ammonium fluoride (NH_4F) and 1.681g urea (denoted as S-2) were mixed together with deionized water by magnetic stirring to form 70ml pink transparent solution. Then the solution was transformed to a 100 ml Teflon-lined stainless steel autoclave, and a piece of cleaned Ti foil (12 cm^2) was immersed into the solution on the liner of the autoclave. The autoclave was maintained at 120 ^oC for 5 h. The substrate was washed with deionized water and ethanol for several times after the device cooled to room temperature. Before the calcination, the substrate was dried in a vacuum oven at 80 ^oC for 5 h, then the substrate was annealed at 350 ^oC under air for 2 h. For comparison, another sample and their corresponding conditions are summarized in Table 1. S-1 and S-2 represent two typical Co_3O_4 NWs with different dimensions synthesized via different concentration of precursors.

Table 1 Summary of the synthesis conditions for Co_3O_4 NWs

Sample	Temperature(^oC)	Concentration(mol/L)			Time(h)
		$Co(NO_3)_2$	NH_4F	urea	
S-1	120	0.04	0.08	0.20	5
S-2	120	0.08	0.16	0.40	5

Preparation of Co_3O_4/TiO_2 nano-coaxial hybrids

In a typical LPD synthesis, taking S-2 for instance, 5ml $(NH_4)_2TiF_6$ (0.2M) and 5ml H_3BO_3 (0.4M) were mixed, forming a homogeneous transparent solution. The substrate prepared after the first step was immersed into the solution at 20 ^oC for 30 min. Remarkably, the morphology and thickness of the TiO_2 coating can be controlled through the adjustment of reaction time and temperature. Here we fixed the reaction temperature at 20 ^oC under water bath. Basically; the thickness of the TiO_2 coating is in positive correlation with the LPD time and temperature.

The final substrate was washed with deionized water and ethanol for several times before being dried in a vacuum oven at 80 ^oC for 5 h, then the dried sample was annealed under air at 550 ^oC for 3 h with a heating rate 5 ^oC/min.

Material characterization

The phase of the products (S-2 was chosen as the representative for testing) was analyzed by X-ray diffraction (XRD) (Rigaku D/Max-2400) with Cu Kα radiation at a scanning rate of 6°/min. Field-emission scanning electron microscopy (FE-SEM, Hitachi, S-4800) and transmission electron microscopy (TEM, JEOL 2010 F) were used to observe the morphology. Element distribution was investigated by the adjunctive energy dispersive X-ray spectroscope (EDS) of the TEM device. X-ray photo electron spectroscope (XPS) measurements were performed on VG ESCALABMKII to study the surface electronic state and the composition of the nanohybrids. The mass loading of the active materials was calculated by gravimetric method with a AB135-S (METTLER, Switzerland), based on the weight of Ti foil or thin-film samples such as Co_3O_4 NWs on Ti substrate after calcination and the Co_3O_4/TiO_2 nanohybrids on Ti substrate after calcination.

Electrochemical behaviors were investigated in CR2025 coin cells. The cells were assembled with the nanohybrids, electrolyte, lithium foil and Celgard 2300 membrane in an Ar filled glove box (MB-10-G with TP170b/mono, MBRAU). 1M $LiPF_6$/EC-DEC(1:1 by vol.) was used as the electrolyte. Each cell was aged for 10 h at room temperature before being tested. The galvanostatic charge-discharge measurements were carried out in a battery test system (NEWARE BTS-610, Neware Technology Co., Ltd., China) at room temperature. The cut-off voltage window for various rate test was between 0.01V and 3.0V (*vs.* Li/Li^+). Cyclic voltammetry (CV) test was carried out on a CHI 1100a electrochemical workstation at a scanning rate of 0.1mV/s between 0.01 and 3.0 V (*vs.* Li/Li^+). Pure Co_3O_4 anode was also assembled and tested for comparison.

Results and discussion

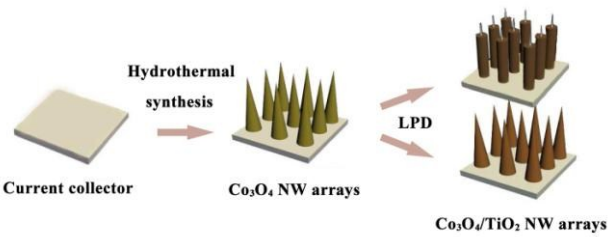

Fig. 1 Schematic illustration for the formation process.

Co_3O_4/TiO_2 nanohybrids were fabricated through a layer by layer procedure. Fig. 1 schematically illustrates the formation process. Two different morphologies can be achieved by adjusting the LPD reaction parameters. Obviously, the morphology of the hybrids depends on the relative content of the components, thus a different performance is achieved. Co_3O_4 NWs synthesized via hydrothermal method served as the backbone for TiO_2 coating and can enhance adhesion to the current collector. The nano-coaxial architecture exhibits a relatively high specific capacity due to the enhanced cycling stability of Co_3O_4 induced by TiO_2 coating.

The phase composition and structure of the samples were investigated by XRD, as shown in Fig. 2a. In detail, sample α represents Ti foil while sample β represents Co_3O_4 NWs on Ti foil and sample γ represents Co_3O_4/TiO_2 nanohybrids (the LPD is conducted under 20 ^oC for 30 min). The diffraction peaks in pattern α can be indexed to Ti substrate. The XRD patterns not only verify the existence of Co_3O_4 but also prove its good crystallinity due to the intense peaks (JCPDS card No. 42-1467), comparing patterns β and α in Fig. 2. However, pattern γ shows the existence of TiO_2 anatase phase (JCPDS card No. 21-1272), yet the peaks are much weaker than Co_3O_4 and Ti, which may be ascribed to its low amount or poor crystallinity. The EDS

analysis shown in Fig. 2b clearly reveals the elements in the nanohybrids. Copper element comes from the copper grid and O element can be omitted due to the poor accuracy of the device for light elements.

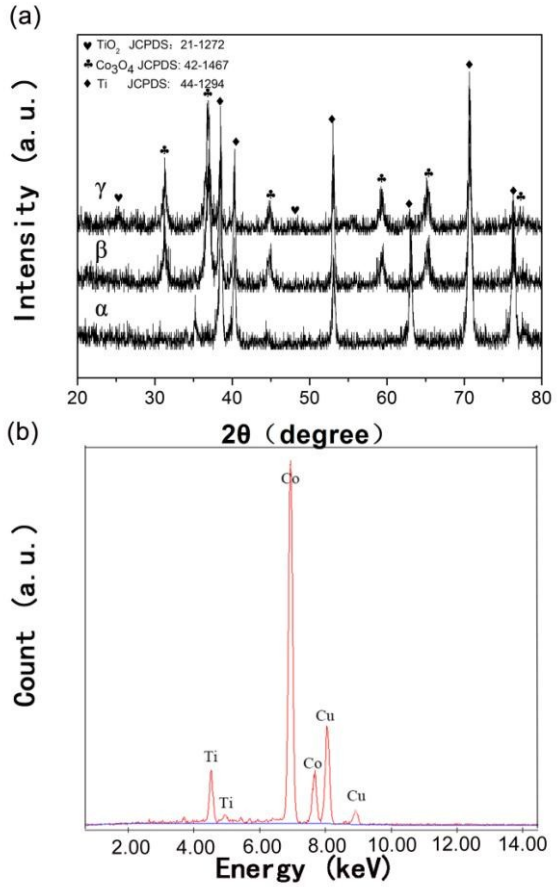

Fig. 2 (a) XRD patterns of (α) Ti foil, (β) Co_3O_4 NWs on Ti foil, (γ) Co_3O_4/TiO_2 nanohybrids on Ti foil; (b) EDS of the Co_3O_4/TiO_2 nanohybrids from S-2.

XPS was also carried out to further estimate the surface electronic state and the composition of the nanohybrids. The O 1s, Ti 2p, and Co 2p XPS spectra for as-formed nano-coaxial structure are exhibited. The core level spectra of Co 2p in Fig. 3a shows two major peaks at 779.9 and 795.1 eV, which are assigned to the Co 2p3/2 and Co 2p1/2 peaks, respectively. The shake-up satellite peaks in the Co 2p spectra further suggest the formation of the Co_3O_4 phase.[34] Fig. 3b presents the XPS spectra of Ti 2p doublet peaks; the binding energies of Ti 2p1/2 and Ti 2p3/2 are observed at approximately 464.8 eV and 459.1 eV with a spin-orbital doublet splitting of 5.7 eV, which is typical of Ti^{4+} in an octahedral environment.[34] The binding energy component observed at 530.0 eV is attributed to the O^{2-} forming oxides with titanium and cobalt in Fig. 3c.

After the coating of TiO_2 film through LPD, Co_3O_4 NWs were covered by TiO_2 shell uniformly. Fig. 4a and b show the images of pure Co_3O_4 NWs and the nano-coaxial hybrids with LPD time of 15 min, respectively. Fig. c and d show SEM in different magnification of Co_3O_4/TiO_2 nanohybrids when the LPD time varied from 15 min to 30 min. Obviously, LPD method shows the significant reaction activity, forming a nano-coaxial architecture. Comparing b and c, we can also detect that long reaction time may bring about more TiO_2 coating; other causes may lead to higher reaction temperature and a relatively slender size of the Co_3O_4 NW core. From the high magnification SEM inset d, we could find that TiO_2 is composed of numerous particles to form a porous nano-pie, which may be conducive to the infiltration of electrolyte and de-intercalation of Li^+. Consequently, we conclude that so much TiO_2 coating leads to a relatively low specific capacity. (Fig. S3, Electronic Supplementary Information)

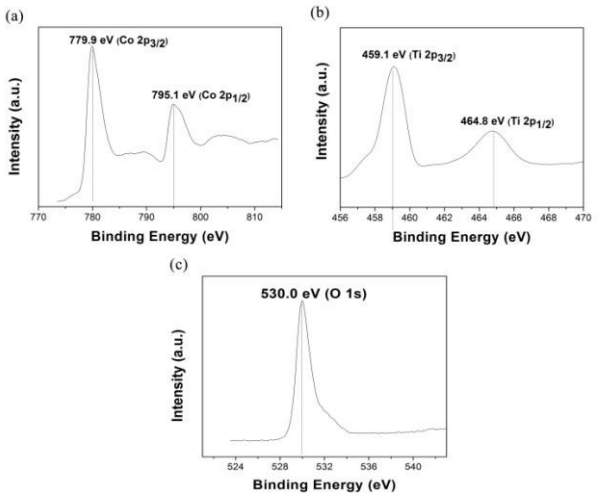

Fig. 3 XPS spectra of (a) Co 2p, (b) Ti 2p, (c) O 1s regions of Co_3O_4/TiO_2 nanohybrids.

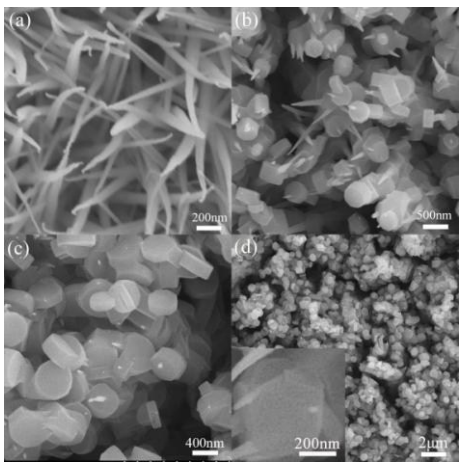

Fig. 4 FESEM of S-1 and Co_3O_4/TiO_2(LPD temperature is 40 °C): (a) pristine Co_3O_4 NWs; (b) Co_3O_4/TiO_2 nanohybrids attained by LPD for 15 min; (c) Co_3O_4/TiO_2 nanohybrids attained by LPD for 30 min; (d) Low and high magnification SEM of the Co_3O_4/TiO_2 hybrids (LPD 30 min).

Fig. 5a shows FESEM of Co_3O_4 NWs from S-2 of which the

diameter reaches 120 nm (Fig. S1a, Electronic Supplementary Information). In Fig. 5b, from the side view of the Co_3O_4 NWs, it can be confirmed that these NWs contact well with the substrate. Furthermore, under our experimental conditions, Ti foil with dimensions up to 12cm^2 could be uniformly coated with the samples whose thickness reaches 6.7μm. Actually, over-thick Co_3O_4 NW array has an adverse impact on the cycling stability of the electrode, but it is favorable to meet the demands of future high-power and high energy density in both thin-film microbatteries and conventional batteries,[3] thus TiO_2 coating shows significance in improving its cyclic stability while maintaining a high specific capacity. For comparison, the SEM images of S-1 given in Fig. S1b exhibit a relatively short NW length and small diameter. Compared with Fig. 4, these core-shell nanohybrids have a much thinner shell layer as a result of lower LPD temperature (20 ^oC). We could unanimously infer that the samples (Fig. 5c and d) still maintain the NW array morphology after the LPD and subsequent calcination, which favors the electrochemical performance improvement for the superiority of 1D NW architecture and the coating effect of thin TiO_2 shell.

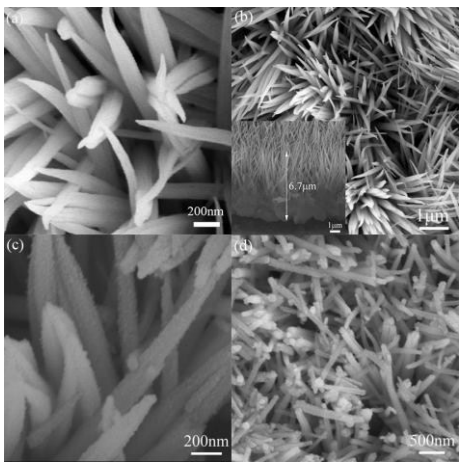

Fig. 5 FESEM of S-2 and Co_3O_4/TiO_2: (a), (b) high-magnification and low-magnification images of the Co_3O_4 NWs, respectively (sideview inset b); (c), (d) high-magnification and low-magnification images of the Co_3O_4/TiO_2 hybrids.

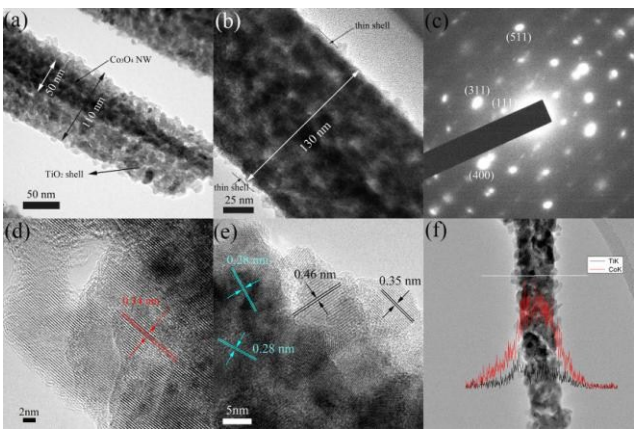

Fig. 6 TEM images of (a), Co_3O_4/TiO_2 nanohybrids (S-1); (b) Co_3O_4/TiO_2 nanohybrids (S-2); (c) SAED pattern of the core; (d) HRTEM image of the fringe parts of the Co_3O_4/TiO_2 nanohybrids (S-1); (e) HRTEM image of the fringe parts in the Co_3O_4/TiO_2 nanohybrids (S-2); (f) EDS line scan across the middle part of a single core-shell NW.

Fig. 6a and b exhibit typical TEM images for the nanohybrids, from which we could clearly see the "core-shell" nanostructure. The Co_3O_4 NW core is composed of numerous interconnected nanoparticles, and its surface seems to be uniformly coated with TiO_2, whose thickness differs depending upon experimental conditions. Both images in Fig. 6a and Fig. 6b show the coaxial core-shell morphology, yet in Fig. 6a the diameter of the core approximates 50 nm while in Fig. 6b the diameter of the core approximates 120 nm. However, the two core-shell nanohybrids possess similar diameter on the whole due to different thickness of the TiO_2 shell, with (a) about 110 nm and (b) about 130nm. Actually the thickness can be adjusted by controlling the synthesis condition of the LPD process.

The LPD process consists of a ligand exchange equilibrium reaction of the metal-fluoro complex ions (Eq.1) and F^- ions consuming reaction by boric acid as a F^- scavenger (Eq.2)

$$(TiF_6)^{2-} + 2H_2O \leftrightarrow TiO_2 + 6F^- + 4H^+ \quad (1)$$

$$H_3BO_3 + 3H^+ + 4F^- \leftrightarrow BF_4^- + 3H_2O \quad (2)$$

H_3BO_3 reacts readily with F^- to form more stable BF_4^-, which facilitates the consumption of non-coordinated F^-. In this process, it is possible to form a TiO_2 thin film on the substrate which is immersed in the solution for deposition.[28,31,32]

The selected area electron diffraction (SAED) pattern of the core is shown in Fig. 6c, whose distinct diffraction spots indicate its good crystallinity. This is consistent with the XRD experimental results, which favors the electron transport.[12] HRTEM analysis from the edge parts of the core-shell nanohybrids in (d) and (e) shows the lattice fringe with lattice spaces of 0.28nm, 0.46nm and 0.34(0.35) nm, which match well with (220), (111) crystal plane of Co_3O_4 and (101) crystal plane of TiO_2, respectively. Furthermore, from the line scan result of EDS (along the white line in Fig. 6f, across the middle part of one core-shell NW); we can conclude that Ti element is uniformly distributed while Co element shows a curve like Gaussian distribution owing to the core-shell nano-coaxial architecture.

Fig. 7a shows the CV curves of the Co_3O_4 NWs electrode. One cathodic peak is observed at 0.77 V in the first cycle, which corresponds to the electrochemical reduction reaction of Co_3O_4 and formation of the solid electrolyte interphase (SEI).[29,30] One anodic peak is recorded at around 2.08V, which corresponds to the oxidation reaction of Co_3O_4. In the subsequent cycles, only one cathodic peak could be observed around 1.07V, and the position of the anodic peak shifts a little to 2.01V. Theoretically, the formation of Co and Li_2O and the re-formation of Co_3O_4 can be described by the following electrochemical conversion reaction:[29,30]

$$Co_3O_4 + 8Li^+ + 8e^- \leftrightarrow 3Co + 4Li_2O \quad (3)$$

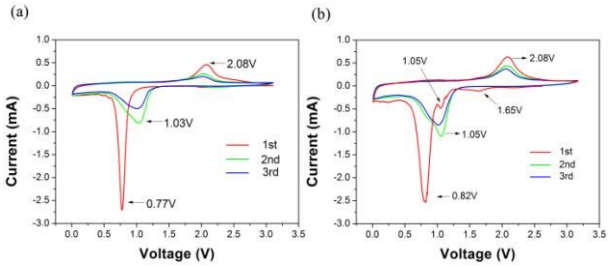

Fig. 7 (a) CV curves of Co_3O_4 NWs electrode (S-2), (b) Co_3O_4/TiO_2 core-shell nanohybrids (S-2).

Fig. 7b shows the CV curves of the hybrid electrode. In the first cycle, two pronounced reduction peaks are observed at 0.82 V and 1.05 V, which can be attributed to the formation of Li_2O, as well as the SEI film.[29] There is a small reduction peak at 1.65V, which may be caused by the shell TiO_2 reaction when Li^+ is inserted in.[25,35] As presented in Eqn. 4 below, the reaction between Li^+ and TiO_2 causes one pair of redox peaks located at 1.65V and 2.08V, respectively. The subsequent well-defined oxidation peaks are observed at 2.08V, indicating the extraction of Li^+. These results nearly coincide with the voltage plateaus in the galvanostatic discharge-charge curve (Fig. 8b). CV curves of the S-1 electrode are shown in Fig. S2, from which we can see a big difference in current intensity but similar numbers, shape and position of the redox peaks. Typically, the S-1 electrode with a thinner layer of active materials shows better reaction kinetics due to the shorter transport length.

$$TiO_2 + x(Li^+ + e^-) \leftrightarrow Li_xTiO_2 (0<x<1) \quad (4)$$

Galvanostatic discharge-charge tests were measured with a voltage cut-off window of 0.01-3.0V. Fig. 8a-c shows the voltage profile, cycling behavior, and coulombic efficiency of the self-supporting Co_3O_4/TiO_2 electrode and pure Co_3O_4 NWs electrode (S-2) at a current density of 0.24 A/g. The plots of different capacities with voltage for pure Co_3O_4 electrode and the hybrid electrode are inserted into Fig. 8a and b, respectively. Obviously, pure Co_3O_4 electrode displays a bad cycling stability of which the discharge specific capacity decayed greatly from initial 1108mAh/g to 110mAh/g after 50 cycles. In contrast, Co_3O_4/TiO_2 nanohybrids exhibit a much better cycling stability and attain a relatively high discharge capacity of 928mAh/g after 50 cycles. As for the coulombic efficiency, we can notice that the nanohybrids has a much better and more stable characteristics (initial coulombic efficiency reaches 78% and maintains over 98% after 8 cycles) than pure Co_3O_4 electrode. This may be due to the more stable electrode architecture and SEI layer of the core-shell nanohybrids. Fig. 8d exhibits the comparison of the rate capability between the two electrodes. For the core-shell nanocomposite electrode from S-2, the mass of the active material is 0.83-0.90 mg/cm^2. While for pure Co_3O_4 electrode, the mass of Co_3O_4 approximates 0.80 mg/cm^2. Remarkably, it can be found that core-shell nanohybrids shows better cycling stability and can attain a relatively high areal capacity of about 777 μAh/cm^2 after 50 cycles (not shown here). But what cannot be denied is that core-shell nanohybrids exhibits a relatively low initial specific discharge capacity, compared to pure Co_3O_4 NWs electrode. Usually, carbon coating or the composition with other inert materials in anode architecture design will lead to specific capacity loss. For S-1, with a thick shell, the specific capacity of the core-shell architecture decreases while the cycling stability improves, as it remained 529 mAh/g after 400 cycles at a current density of 0.33 A/g (Fig. S3a, Electronic Supplementary Information). We have provided the rate capability of Co_3O_4 NWs and Co_3O_4/TiO_2 nanohybrids from S-1 in Fig. S3. It is notable that both nanohybrids (from S-1 and S-2) show an activation process as the specific capacity increases with cycle-index during the early stage. On one hand, activation process is a common phenomenon for MO_x-based LIBs;[10] On the other hand, here in our core-shell architecture, TiO_2 may decrease the initial discharge capacity because of its coating effect. Usually, nanocomposite electrodes tend to exhibit excellent cyclic stability as aggregation of the active materials is retarded and the outer layer can reduce the pulverization of the inner material during the cycling.[38] In brief, the improved lithium-storage performance of the Co_3O_4/TiO_2 NWs can be attributed to a large contact area between the anodes and the electrolyte which can facilitate the insertion/extraction of Li^+, the intricate core-shell nanowire architecture as free-standing nanowire morphology can supply efficient electron-transport pathways and accommodate the strain caused by repeated lithium insertion/extraction and the coating of TiO_2 thin shell, which exhibits excellent performance such as small volume change, good cycling stability and robust crystal structure to electrolyte when used as anode material for LIBs, thus the enormous volume change and internal strain are accommodated to restrict cracking.[40-42]

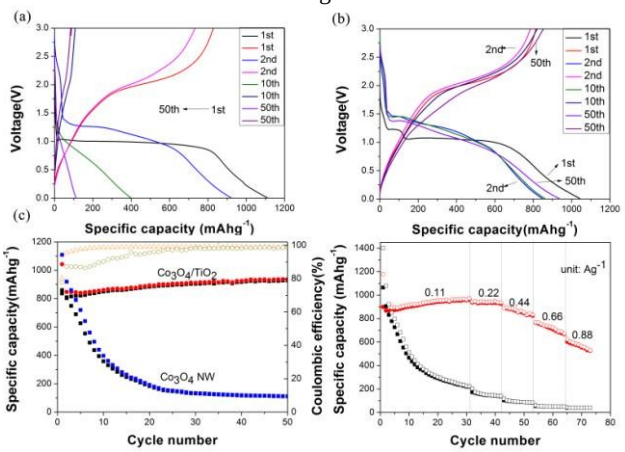

Fig. 8 (a) Voltage-specific capacity profiles of pure Co_3O_4 NWs electrode and (b) voltage-specific capacity profiles of core-shell nanohybrids at 0.24 A/g, (c) Cycling performance and coulombic efficiency of the core-shell nanohybrids and pure Co_3O_4 NWs; (d) Rate capability of the core-shell nanohybrids and pure Co_3O_4 NWs at various current rates.

In addition, to determine whether the morphology of NWs electrode had broken down after repeated lithiation/delithiation, the cells were disassembled after 200 cycles for SEM characterization of the electrodes as shown in Fig. S4. Obviously, pulverization and exfoliation of the Co_3O_4 film are observed over the current collector, which would be regarded as the main cause of the capacity decay. However, the morphology of the hybrids electrode shows much less exfoliation which demonstrates good

structural integrity during many cycles. The TiO_2 shell may serve as a mechanical constraining and reinforcing layer that could effectively accommodate the enormous volume change and internal strain to restrict cracking.[42] Finally, the hybrids electrode has not disintegrated like the pure Co_3O_4 NWs does, which proves the advantage of the core-shell nanoarchitecure and TiO_2 coating. Still, there is much more work to be done such as method to improve the bad conductivity of TiO_2 coating while maintaining its excellent electrochemical performance and the charging mechanism of lithium ions between Co_3O_4 and TiO_2 phases.

Conclusions

In summary, nano-coaxial Co_3O_4/TiO_2 arrays are successfully synthesized in situ through a facile and extensive LPD strategy by using vertical Co_3O_4 NWs as the core material on Ti foil. From the physical characterizations, it can be found that small-sized TiO_2 nanoparticles are deposited onto the Co_3O_4 NWs to form an ultra-thin TiO_2 layer in control. When used as anodes for lithium storage, the nanohybrids presents remarkable areal capacity or specific capacity and good cycling stability, which are assumed to derive from the intricate core-shell nanoarchitecture and the coating effect of TiO_2, including improved mechanical/chemical stability and good strain accommodation. It is also anticipated that the synthetic strategy presented could be applied to fabricate and optimize other core-shell nanoarchitectures for high performance lithium storage devices.

Acknowledgements

This work was supported by the National Basic Research Program of China (973 Program) (2013CB934001), National Natural Science Foundation of China (51074011 and 51274017), National 863 Program of China (2011AA11A257, 2012AA052201, 2012AA110102 and 2013AA050904), and International S&T Cooperation Program of China (2012DFR60530).

References

1 A. S. Arico, P. Bruce, B. Scrosati, J. M. Tarascon and W. Van Schalkwijk, *Nat. Mater*., 2005, **4**, 366-377.
2 Y. P. Wu, E. Rahm and R. Holze, *J. Power Sources*, 2003, **114**, 228-236.
3 K. Sun, T. S. Wei, B. Y. Ahn, J. Y. Seo, S. J. Dillon and J. A. Lewis, *Adv. Mater*., 2013, **25**, 4539-4543.
4 T. Djenizian, I. Hanzu and P. Knauth, *J. Mater. Chem.*, 2011, **21**, 9925-9937.
5 B. L. Ellis, P. Knauth and T. Djenizian, *Adv. Mater*., 2014, **26**, 3368-3397.
6 H. Huang, W. Zhu, X. Tao, Y. Xia, Z. Yu, J. Fang, Y. Gan and W. Zhang, *ACS Appl. Mater. Interfaces*, 2012, **4**, 5974-5980.
7 H. Fang, S. C. Zhang, W. B. Liu, Z. J. Du, X. M. Wu and Y. L. Xing, *Electrochim. Acta*, 2013, **108**, 651-659.
8 L. Zhuo, Y. Wu, J. Ming, L. Wang, Y. Yu, X. Zhang and F. Zhao, *J. Mater. Chem. A*, 2013, **1**, 1141-1147.
9 H. Y. Sun, Y. G. Liu, Y. L. Yu, M. Ahmad, D. Nan and J. Zhu, *Electrochim. Acta*, 2014, **118**, 1-9.
10 C. Peng, B. Chen, Y. Qin, S. Yang, C. Li, Y. Zuo, S. Liu and J. Yang, *ACS Nano*, 2012, **6**, 1074-1081.
11 X. Xia, J. Tu, Y. Zhang, X, Wang, C. Gu, X. B. Zhao and H. J. Fan, *ACS Nano*, 2012, **6**, 5531-5538.
12 J. P. Liu, J. Jiang, C. W. Cheng, H. X. Li, J. X. Zhang, H. Gong and H. J. Fan, *Adv. Mater*., 2011, **23**, 2076-2081.
13 D. Kong, J. Luo, Y. Wang, W. Ren, T. Yu, Y. Luo, Y. Yang and C. Cheng, *Adv. Funct. Mater*., 2014, **24**, 3815-3826.
14 X. Y. Xue, S. Yuan, L. L. Xing, Z. H. Chen, B. He and Y. J. Chen, *Chem. Commun*., 2011, **47**, 4718-4720.
15 W. Mei, J. Huang, L. Zhu, Z. Ye, Y. Mai and J. Tu, *J. Mater. Chem*., 2012, **18**, 9315-9321.
16 L. Zhan, S. Q. Wang, L. X. Ding, Z. Li and H. H. Wang, *Electrochim. Acta*, 2014, **135**, 35-41.
17 X. Su, Q. L. Wu, X. Zhan, J. Wu, S. Y. Wei and Z. H. Guo, *J. Mater. Sci.*, 2012, **47**, 2519-2534.
18 P. Kubiak, T. Froschl, N. Husing, U. Hormann, U. Kaiser, R. Schiller, C.K. Weiss, K. Landfester and M. Wohlfahrt-Mehrens, Small, 2011, **7**, 1690-1696.
19 Z. Wang and X. W. Lou, *Adv. Mater*., 2012, **24**, 4124-4129.
20 Y. Lan, X. P. Gao, H. Y. Zhu, Z. F. Zheng, T. Y. Yan, F. Wu, S. P. Ringer and D. Y. Song, *Adv. Funct. Mater*., 2005, **15**, 1310-1318.
21 Y. S. Hu, L. Kienle, Y. G. Guo and J. Maier, *Adv. Mater.*, 2006, **18**, 1421-1426.
22 T. Beuvier, M. Richard-Plouet, M. M. L. Granvalet, T. Brousse, O. Crosnier and L. Brohan, *Inorg. Chem*., 2010, **49**, 8457-8464.
23 S. H. Liu, H. P. Jia, L. Han, J. L. Wang, P. F. Gao, D. D. Xu, J. Yang and S. N. Che, *Adv. Mater*., 2012, **24**, 3201-3204.
24 X. Xin, X. Zhou, J. Wu, X. Yao and Z. Liu, *ACS Nano*, 2012, **6**, 11035-11043.
25 D. Deng, M. G. Kim, J. Y. Lee and J. Cho, *Energy Environ. Sci.*, 2009, **2**, 818-837.
26 S. K. Cheah, E. Perre, M. Rooth, M. Fondell, A. Harsta, L. Nyholm, M. Boman, T. Gustafsson, J. Lu, P. Simon and K. Edstrom, *Nano Lett.*, 2009, **9**, 3230-3233.
27 E. M. Lotfabad, P. Kalisvaart, A. Kohandehghan, K. Cui, M. Kupsta, B. Farbod and D. Mitlin, *J. Mater. Chem. A*, 2013, **8**, 2504-2516.
28 S. Yamanaka, H. Muta, K. Kurosaki, M. Uno and T. Hamaguchi, *J. Alloy. Compd.*, 2004, **373**, 312-315.
29 Y. Li, B. Tan and Y. Wu, *Nano Lett*., 2007, **8**, 265-270.
30 Y. Fu, X. Li, X. Sun, X. Wang, D. Liu and D. He, *J. Mater. Chem*., 2012, **34**, 17429-17431.
31 J. Liu, K. Song, P. A. van Aken, J. Maier and Y. Yu, *Nano lett.*, 2014, **14**, 2597-2603.
32 C. F. Yen and M. K. Lee, *J. Electrochem. Soc.*, 2011, **158**, G43-G46.
33 J. Jiang, Y. Y. Li, J. P. Liu, X. T. Huang, *Nanoscale*, 2011, **3**, 45-58.
34 Y. Q. Liang, Z. D. Cui, S. L. Zhu, Z. Y. Li, X. J. Yang, Y. J. Chen, J. M. Ma, *Nanoscale*, 2013, **5**, 10916-10926.
35 X. M. Wu, S. C. Zhang, L. L. Wang, H. Fang, Y. H. Ling, Z. H. Huang, J. Mater. Chem., 2012, **22**, 11151-11158.
36 J. Y. Liao, V. Chabot, M. Gu, C. M. Wang, X. C. Xiao, Z. W. Chen, *Nano Energy*, 2014, **9**, 383-391.

37 J. Y. Liao and A. Manthiram, *Adv. Energy Mater*., 2014, **4**, 1400403.
38 J. Jiang, J. S. Luo, J. H. Zhu, X. T. Huang, J. P. Liu and T. Yu, *Nanoscale*, 2013, **5**, 8105-8113.
39 N. N. Wang, J. Yue, L. Chen, Y. T. Qian and J. Yang, *ACS Appl. Mater. Interfaces*, 2015, **7**, 10348-10355.
40 Q. Wang, J. Sun, Q. Wang, D. A. Zhang, L. L. Xing, X. Y. Xue, Chem. Asian J, 2014, 9, 3299 – 3306.
41 Q. Wang, D. A. Zhang, Q. Wang, J. Sun, L.L. Xing, X.Y. Xue, Electrochim. Acta, 2014, 146, 411-418.
42 Q. Wang, J. Sun, Q. Wang, D.A. Zhang, L.L. Xing, X.Y. Xue, J. Mater. Chem. A, 2015, 3, 5083-5091.

Facile shape control of nano-coaxial Co_3O_4/TiO_2 arrays and the effect of the microstructure on lithium storage capability

Tao Qi, Shichao Zhang,* Xiaomeng Wu, Yalan Xing, Guanrao Liu and Yanbiao Ren

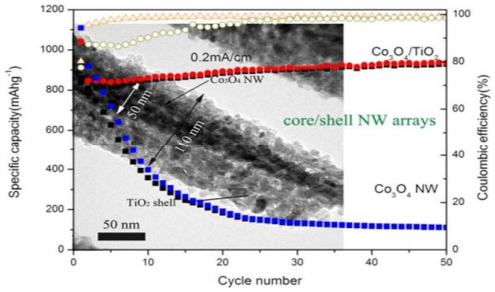

Co_3O_4/TiO_2 nanohybrids fabricated via a layer by layer procedure have exhibited excellent electrochemical performance.